Characterization of the cloud microphysical and optical properties and aerosol-cloud interaction in the Arctic from in situ ground-based measurements during the CLIMSLIP-NyA campaign, Svalbard

Gwennolé Guyot, Frans Olofson, Peter Tunved, Christophe Gourbeyre, Guy Fevbre, Regis Dupuy, Christophe Bernard, Gérard Ancellet, Kathy S. Law, Boris Quennehen, et al.

Atmos. Chem. Phys. Discuss., https://doi.org/10.5194/acp-2017-672
Manuscript under review for journal Atmos. Chem. Phys.
Discussion started: 1 November 2017

Atmospheric Chemistry and Physics Discussions

Characterization of the cloud microphysical and optical properties and aerosol-cloud interaction in the Arctic from in situ ground-based measurements during the CLIMSLIP-NyA campaign, Svalbard

Gwennolé GUYOT[1], Frans OLOFSON[1], Peter TUNVED[2], Christophe GOURBEYRE[1], Guy FEVBRE[1], Régis DUPUY[1], Christophe BERNARD[1], Gérard ANCELLET[3], Kathy LAW[3], Boris QUENNEHEN[4], Alfons SCHWARZENBOECK[1], Kostas ELEFTHERIADIS[5], Olivier JOURDAN[1]

[1] Laboratoire de Météorologie Physique (LaMP), Université Blaise Pascal (UBP), OPGC, CNRS UMR 6016, Clermont-Ferrand, France
[2] Department of Applied Environmental Science (ITM), Stockholm University, Stockholm, Sweden
[3] Laboratoire Atmosphère, Milieux et Observations Spatiales (LATMOS), IPSL, UPMC, CNRS UMR 8190, Paris
[4] Laboratoire de Glaciologie et Géophysique de l'Environnement (LGGE), Université Grenoble Alpes/CNRS, 38041 Grenoble, France
[5] Environmental Radioactivity Laboratory, Institute of Nuclear and Radiological Science & Technology, Energy & Safety, Attiki, Greece

Abstract

This study will focus on cloud microphysical and optical characterization of three different types of episodes encountered during the ground based CLIMSLIP-NyA campaign performed in Ny-Alesund, Svalbard: the Mixed Phase Cloud (MPC), snow precipitation and Blowing Snow (BS) events. These in situ cloud measurements will be combined with aerosol measurements and air mass backtrajectory simulations to qualify and parameterize the arctic aerosol cloud interaction and to assess the influence of anthropogenic pollution transported into the Arctic.

The results show a cloud bimodal distribution with the droplet mode at 10 µm and the crystal mode centered at 250 µm, for the MPC cases. The precipitation cases presents a crystal distribution centered around 350 µm with mostly of dendritic shape. The BS cases show a higher concentration but smaller crystals, centered between 150 and 200 µm, with mainly irregular crystals.

A "polluted" case, where aerosol properties are influenced by anthropogenic emission from Europe and East Asia, was compared to a "clean" case with local aerosol sources. These anthropogenic emissions seem to cause higher Black Carbon, aerosol and droplet concentrations, a more pronounced accumulation mode, smaller droplet sizes and a higher activation fraction F_a. Moreover, the activation diameter decreases as the droplet diameter increases and F_a increases showing that smaller particles are activated and droplets grow when the aerosol number decreases. This is in agreement with the first (Twomey) and second (Albrecht) aerosol indirect effect. The quantification of the variations of droplet concentration and size leads to *IE* (Indirect Effect) and *NE* (Nucleation Efficiency) coefficients values around 0.2 and 0.43, respectively. These values are close to those found by other studies in the arctic

region which confirms these parameterizations of arctic aerosol-cloud interaction in climate models.

1 Introduction

The Arctic is a region where the surface warming is faster than the global average warming, associated with, in particular, a rapid melting of the sea ice in summer (Vaughan et al., 2013). This is the so-called arctic amplification. Several studies indicate that the arctic warming is mainly of anthropogenic origin (e.g., Mc Guire et al., 2006, Serreze and Francis, 2006). The arctic amplification is due to several positive feedbacks specific to the Arctic, the most important being the sea ice melting feedbacks (Screen and Simmonds, 2010). Changes in atmospheric and oceanic circulation, cloud properties (especially cloud cover) and atmospheric water vapor amount are highly expected but their quantification remains uncertain. Specially, the effects of clouds dominate the intermodal standard deviation of a temperature rise due to an increase of atmospheric CO_2 concentration (Dufresne and Bony, 2008).

Recent remote sensing studies have shown that the clean and stable arctic atmosphere is characterized by a high occurrence of mixed phase clouds (MPC) all year long, except in winter and early spring when ice clouds are important (Mioche et al., 2015). However, the Svalbard region is an exception where MPC are the most frequent cloud independent of season (Mioche et al., 2015). Moreover, the altitude of the MPC is highly dependent of the height of the inversion layer. The frequently occurring situation with a stable atmosphere and the low level pronounced inversion layer promotes low level clouds of stratus form (Curry et al., 1996). The arctic MPC are composed of a liquid layer on top and below which is located the mixed phase where ice crystals take form (Gayet et al., 2009). If the crystals grow enough, a precipitation layer is produced below the cloud. The dynamics together with possible surface coupling and advection are essential to maintain the MPC during several days (Morrison et al., 2012). This structure results from a complex network of interactions between numerous local and larger scale processes that complicates the understanding of the MPC properties evolution and its impact on arctic climate (Morrison et al., 2012). In the Arctic, the umbrella effect is not necessarily dominant compared to the cloud greenhouse effect (Quinn et al., 2008), which suspects that clouds play an important role in the arctic amplification. Several studies have revealed that MPCs have a large impact on the surface radiative flux in the Arctic (e.g. Kay et al., 2012, Wendisch et al., 2013).

Arctic cloud properties are linked to aerosol properties since they can act as Cloud Condensation Nuclei (CCN) or Ice Nuclei (IN). Thus, aerosol seasonal variability and transport from lower latitudes play a role in cloud properties evolution. Studies have shown an arctic annual mean aerosol concentration half that for mid-latitudes. The stable atmosphere and the dark winter promote growth by coagulation/coalescence of the particles, i.e. an increase in size and decrease in concentration, with dominant accumulation mode (Tunved et al., 2013). When the sun rises during spring, these big particles, which can come from lower latitudes, generate the arctic haze phenomenon (Quinn et al. 2007). The stronger sun light gives rise to increasing photochemical activity associated with new particle formation and a dominant Aitken mode (Engwall et al., 2008). Moreover, the ice melting exposes land surfaces that can act as aerosol sources. Therefore, the aerosol concentration increases until its maximum in summer. These features were observed in Alaska (Quinn et al., 2002) and Svalbard (Tunved et al., 2013), proving that they are representatives of the aerosol properties evolution in the Arctic.

The rapid change in aerosol properties occurring in spring is known to cause changes in arctic cloud properties, the so-called aerosol indirect effect. Increase in aerosol concentration with constant Liquid Water Path (*LWP*) is known to increase cloud droplet concentration and cloud optical thickness but decrease droplet size (Twomey, 1974, 1977), decrease the precipitation efficiency and increase the cloud lifetime (Albrecht, 1989). Also, in a temperature rise scenario, the cloud height is expected to increase (Pincus and Baker, 1994). The impacts of anthropogenic aerosol transported to the Arctic on clouds are not fully understood, but Garrett and Zhao (2006) showed that the cloud emissivity is higher for polluted case, contributing to the arctic warming.

In the case of artic MPC where liquid and ice phases coexist, the aerosol-cloud interaction is complexified by the addition of the ice phase and several interaction mechanisms have been assumed. Lohmann (2002a, 2002b) proposed that an increase in ice nuclei could increase the cloud ice content at the expense of the liquid content. This so-called glaciation indirect effect would mean, as the precipitation is more efficient for the ice phase, a decrease in cloud cover in lifetime. The riming indirect effect predicts a riming efficiency decrease due to the supercooled droplet size decrease. Thus, an increase in Cloud Condensation Nuclei (CCN) could lead to a decrease in Ice Water Content (IWC) and ice particles concentration (Borys et al., 2003). According to the data of the two measurement campaigns ISDAC (Indirect and Semi-Direct Aerosol Campaign) and MPACE (Mixed-Phase Arctic Cloud Experiments), Jackson et al. (2012) found a correlation corresponding to the glaciation effect above the cloud liquid phase but no evidence of the riming effect. Mc Farquhar et al. (2011) showed that the aerosol size is the main parameter to explain the particles activation and that the chemical properties don't determine the ability of an aerosol to act as a CCN, i.e. the Kelvin effect is dominant compared to the Raoult effect in the Arctic.

The work presented here is included in the frame of the project CLIMSLIP (CLimate IMpacts of Short-LIved Pollutants in the polar region). The main objective of this project is to reduce the uncertainties of the radiative forcing due to the anthropogenic emissions of tropospheric ozone, methane and aerosol including Black Carbon (BC). This article will focus on the arctic ground based in situ cloud and aerosol measurement study, performed at the Mount Zeppelin station (474 meters altitude), in Ny-Alesund, Svalbard, performed during spring 2012. First, a classification and characterization of the different types of cases will be presented. Then, a comparison between a polluted and a clean case will be made, based on air masses backtrajectories. In the end, the different aerosol-cloud interactions will be discussed and, if possible, quantified.

2 Site & instrumentation

2.1 Site

The campaign was carried out between February 26 and May 2 at the Mount Zeppelin station (78°56'N, 11°53'E) located south-west of the Ny-Alesund village, Svalbard, at an altitude of 474 meters above sea level. This station presented in Figure 1 was built and is managed by the Norwegian Institute for Air Research (NILU). The Zeppelin observatory is mostly unaffected by local sources and is considered to be within the boundary layer most of the time (Tunved et al., 2013). This station represents remote arctic conditions and is a part of the European observation network ACTRIS (Aerosols, Clouds, and Trace gases Research InfraStructure network). Continuous measurements of atmospheric trace gases and aerosol physical and chemical properties

are performed all year long. The station is also equipped with instruments to measure temperature, humidity and wind speed and direction.
A ceilometer, CL51 model, was installed in the Ny-Alesund village at sea level. This remote sensing instrument is designed to measure the clouds within an altitude range between 0 and 15 km. It uses the technology of a lidar with a laser wavelength at 910 nm. During CLIMSLIP, the ceilometer was used to retrieve the approximate altitude of the mixed phase and the liquid layers and showed good agreement with the microphysical measurements. However, in some cases, fog or an optically thick ice layer prevents the laser beam from penetrating within the cloud system.

Figure 1: Picture of the Mount Zeppelin station (www.npolar.no)

2.2 Instrumentation and data processing

2.2.1 Cloud instrumentation

The cloud ground based instrumentation used during CLIMSLIP-NyA was installed on a measurement pole and is presented in Figure 2. The cloud optical and microphysical properties were thus assessed by three independent instruments: a PMS Forward Scattering Spectrometer Probe (FSSP-100), a Cloud Particle Imager (CPI) and a Polar Nephelometer (PN). They were all connected to the same pump by plastic tubes, leading to the sampling volume indicated on Figure 2. They were operated approximately 2 m above the platform level and mounted on a tilting and rotating mast, allowing them to be moved manually in the prevailing wind direction. The proper alignment of their inlet with the flow was based on the wind direction measurements performed by a mechanical and ultrasonic anemometer.

The FSSP-100 measures the number and the size of particles going through the sampling volume, from the forward scattering of a 632.8 nm wavelength laser beam (Knollenberg, 1981, Dye and Baumgardner, 1984). Using the Mie theory, this instrument is dedicated to droplets. The Particle Size Distribution (PSD) is thus computed in 15 adjustable size classes with uncertainties on the effective diameter and *LWC* of respectively 2 µm and 30 % (Febvre et al., 2012).
The CPI is an imager and takes pictures of the particles when going through the detection volume with 256 grey levels, thanks to a CCD camera with a resolution of 1024 × 1024 pixels. These images allow computing the particles size and so the PSD, but several morphological

parameters are also retrieved and are used to classify the sampled particle in 10 shape categories: spheroid, needle, column, plate, bullet, stellar, graupel, rosette, sideplane and irregular (Lefèvre, 2007). However, a manual classification has been done during the CLIMSLIP campaign due to some malfunctions of the automatic classification. The determination of the IWC is realized according to the Baker and Lawson (2006) and Lawson and Baker (2006) method. The uncertainties on the concentration and the effective diameter are assessed respectively as 50 % and 80 %.

The PN measures the scattering phase function of a set of cloud particles thanks to a 804 nm wavelength laser beam and 56 photodiodes distributed over scattering angles between 3.5° and 172.5° (Gayet et al., 1997). From the scattering phase function can be computed two important integrated optical parameters, the extinction coefficient and the asymmetry parameter with accuracies estimated within 25% and 4%, respectively (Gayet et al., 2002).

The Nevzorov probe is a hot wire device at constant temperature with two captors and an electrical resistor. The particles are vaporized, and an electrical power is provided to the resistor. The resulting power is relied related to the *LWC* and *TWC*, depending on the captor (Korolev et al., 1998). Due to high discrepancies, this instrument was used only for instrumental comparison and data processing analysis and will not be discussed further.

Figure 2: Cloud instrumentation used during CLIMSLIP. Indicated are: particle size range, main cloud properties measured and theoretical sampling speed.

2.2.2 Aerosol instrumentation

The particle inlet at the Mount Zeppelin station is a Whole Air Inlet, which possesses a heating system that prevents the inlet to be filled by ice or frost and to evaporate the condensed water or ice. Thus, all the aerosols (CCN, IN or interstitial) are sampled by the instruments described hereafter. The aerosol sampling covers particles sizes between 3 and 809 nm (Tunved et al., 2013).

The Mount Zeppelin aerosol instrumentation is composed of one Condensation Particle Counter (CPC), one Differential Mobility Particle Sizer (DMPS), one aethalometer and one aerosol nephelometer, which are running continuously throughout the year. The CPC, 3015A model, is a particle counter for aerosol diameters larger than 3 nm. It measures aerosol concentration up to 10^5 particles/cm^3 with an accuracy of 10 % (TSI, 2002). The DMPS is a CPC combined with a Differential Mobility Analyzer (DMA), which allows selecting different size ranges. The aerosol PSD is obtained with 22 diameter classes going from 25 to 809 nm. The aethalometer assesses the Black Carbon (BC) concentration based to the optical extinction of the aerosols

collected on a filter (see Eleftheriadis et al., 2009, for details). The nephelometer measures the aerosol scattering coefficient for three wavelength: 450, 550 and 700 nm (TSI, 2005). During CLIMSLIP, this nephelometer was used with a time resolution of 5 minutes.

2.2.3 Data processing

The three cloud instruments operated at a one Hz resolution. The data processing has followed the conclusions of the cloud instrumentation study presented in Guyot et al. (2015). This paper highlights the biases that can exist between the instruments and the need of an Ensemble of Particles Probe (EPP) to standardize the data. In the case of the CLIMSLIP campaign, such correction was not possible for two reasons not developed further. (1) Strong discrepancies of the EPP Nezvorov probe, probably because of a too low sampling speed. (2) The standardization according to the extinction coefficient of the PN is not consistent with the aerosol data (there are more droplets than CCN). Thus, this study will not provide quantitative results but qualitative ones based on case comparisons and variation studies.
According to Guyot el al. (2015), measurements with an angle between the instruments orientation and the wind direction higher than 30° can modify the PSD due to changes in the sampling conditions. Those measurements were therefore not taken into account for the study. Moreover, the ground based low sampling speed induces low sampling rate, especially for the CPI with values between 0.5 and 20 sampled particles per minute. This doesn't allow us to work on low time resolution scale. To get sufficient particle statistics, the minimum average time resolution will be 1 minute for the FSSP and one day for the CPI.

During the aircraft campaign, a cloud particle can break on impaction with the inlet due to the high sampling speed corresponding to the plane speed. This results in more numerous and smaller droplets or crystals and creates artifacts in the PSD (Rogers et al., 2006). Due to the low sampling speed, ground based measurements has the advantage to avoid this effect, but at the expense of the sampling rate.

3 Identification and characterization of the study cases

3.1 Overview

Several kinds of episodes were met during CLIMSLIP. Figure 3.a shows those episodes with the time series of measured temperature and relative humidity. Thus, according to the ceilometer measurements and observations, we enumerate:

- 4 episodes of sampling of the liquid and mixed phase layer (LMPL) of MPC, on March 11th and 29th and April 27th and 28th.
- 3 cases of sampling of the precipitation layer of MPC, on March 28th and April 14th and 20th.
- 2 occurrences of Blowing Snow (BS), on March 23th and 31th.

Atmos. Chem. Phys. Discuss., https://doi.org/10.5194/acp-2017-672
Manuscript under review for journal Atmos. Chem. Phys.
Discussion started: 1 November 2017

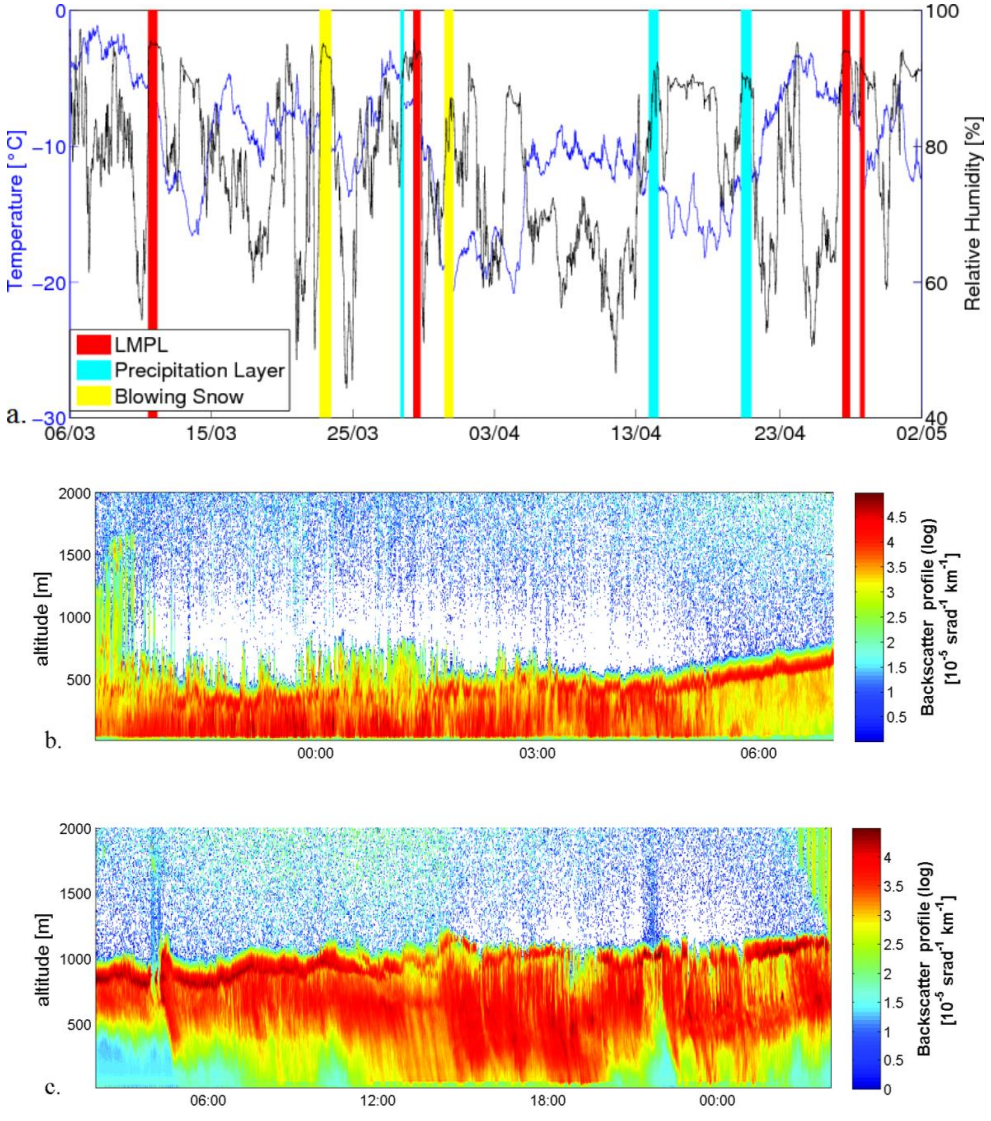

Figure 3: a) Time series of the temperature and relative humidity measured at the Zeppelin station. The different cases are plotted with colored columns. Examples of time series of the ceilometer attenuated backscattered coefficient profile in km^{-1} sr^{-1} for b) MPC case (April 27th) and c) precipitation case (April 14th).

The cases called "LMPL" and "Precipitation layer" both reveal the presence of a MPC, i.e. where cloud in situ instrumentation sampled ice and/or liquid particles. But, in the first case, the ceilometer shows the liquid layer around 500 meters altitude (Figure 3.b). This liquid layer having a very strong extinction coefficient, the ceilometer beam does not go through, what happens above the liquid layer is therefore unknown. On the same time, droplets are sampled by the FSSP. Following the altitude of the cloud, the station is in the liquid layer or the mixed phase layer. These episodes are characterized by relative humidity maximum.

In the second case, the ceilometer locates the liquid layer around 1 km altitude or more (Figure 3.c). No droplets are sampled. The station is so below the mixed layer, within the ice precipitation. This layer has a variable extinction coefficient depending on the crystal density but the laser beam is not completely attenuated. The relative humidity shows high values around 90 % but remains lower than the MPC cases.
Moreover, the temperature varied between -20 to -1 °C, so it remains always below the solidification point, liquid particles were always supercooled droplets. The Blowing Snow episodes will be discussed in annex.

In the following, the LMPL and precipitation layer cases will be microphysically and optically characterized. These characterizations will be useful to determine futures measurements that are not completed with visual observations (e.g., remote sensing measurements). Moreover, combined with other measurement campaign in the Arctic, we hope to increase knowledge about growth processes in low level mixed phase arctic clouds.

3.2 Characterization of the LMPL cases

Arctic MPC can be characterized by a succession of layers with liquid or ice dominance. The phase heterogeneity is both horizontal and vertical. Because of the fixed position of the measuring station, we could not control the location of the measurements within the cloud system. However, a characterization of the mean parameters is possible.

The determination of the thermodynamic phase of a cloud can be based on microphysical and optical criteria. Figure 4 presents the occurrence number of the MPC liquid fraction F_{liq} and the asymmetry parameter g. F_{liq} is computed as :

$$F_{liq} = \frac{LWC_{FSSP}}{(LWC_{FSSP}+IWC_{CPI})} \quad (1)$$

The results show a higher observation frequency for extreme F_{liq} values (close to 0 or 100 %). The minimum frequency is between 20 and 70 %. This means that the low level mixed phase cloud layers are preferentially with liquid or ice dominance for the spatial resolution of our measurements. This confirms the conclusions from the scientific literature (e.g., Gayet and al., 2009; Korolev and Isaac, 2006).
Moreover, g shows a more or less linear relation with F_{liq}. This highlights the relation between the optical properties and the microphysical properties. Therefore, the knowledge of the MPC microphysical properties is a key parameter to reliably assess the radiative transfer in the Arctic. The g variability is significantly larger for F_{liq} below 50 %. This tends to show a more complex optical behavior for ice dominating layers.

Atmos. Chem. Phys. Discuss., https://doi.org/10.5194/acp-2017-672
Manuscript under review for journal Atmos. Chem. Phys.
Discussion started: 1 November 2017

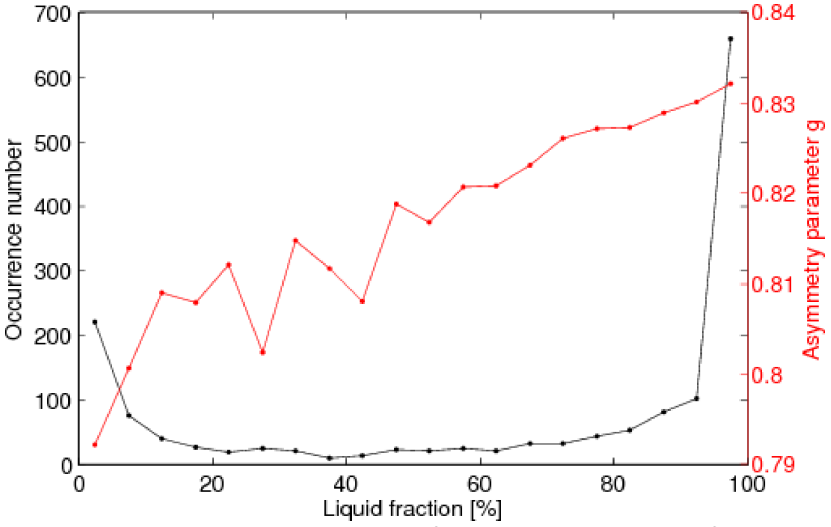

Figure 4: Occurrence number and mean values of g in relation to the liquid fraction F_{liq} for the four LMPL cases. F_{liq} is derived from the CPI and FSSP measurements (see Eq. 1) with 1 minute resolution corresponding to a spatial resolution of 800 meters.

Figure 5 shows the average PSD, from 3 µm to 2.3 mm, obtained with the FSSP and the CPI for the four LMPL cases. The mean F_{liq} is also indicated. The four PSD show similar trends, i.e. two modes centered at 10 µm for droplets and around 250 µm for ice crystals.

According to Costa et al. (2014), these PSD correspond to the coexistence regime characterized by RH_w (relative humidity according to liquid water) and RH_i (relative humidity according to ice) > 100 % and stable coexistence of crystals and supercooled liquid droplets with the droplet PSD 10^6 higher than the crystal PSD. This is opposite to the Bergeron regime where RH_w < 100 % and RH_i > 100 %, so the crystals grow in expense of the droplets (Costa et al., 2014). This reveals that the Wegener-Bergeron-Findeisen process doesn't alone explain the formation and growth of ice crystals.

However, the March 11th and 29th PSDs show differences with the other cases with a high concentration for the smallest CPI classes. This is due to big droplets sampled by the CPI. The FSSP doesn't show such consequent differences in droplet PSD or diameter. We also point out that the absolute values should not be taken into account. Indeed, in addition to instrumental issues (see Guyot el al., 2015), the results and the differences between the cases are largely dependent on the station residence time within the liquid or mixed layer which cannot be controlled. Similar PSDs were observed at the Mount-Zeppelin station by Uchiyama et al. (2013) in 2011. This publication concludes that the liquid/ice distribution is a function of the cloud evolution stage; we highlight here the importance of the station position inside the cloud system for our data analysis.

Atmos. Chem. Phys. Discuss., https://doi.org/10.5194/acp-2017-672
Manuscript under review for journal Atmos. Chem. Phys.
Discussion started: 1 November 2017

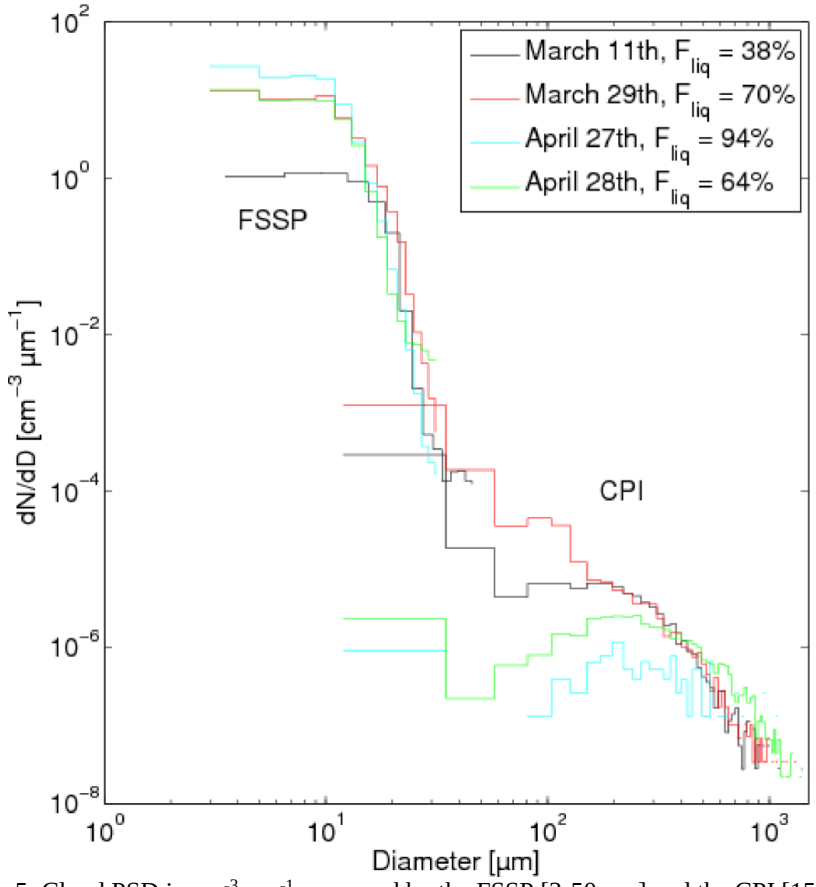

Figure 5: Cloud PSD in cm^{-3} μm^{-1} measured by the FSSP [3-50 µm] and the CPI [15-2300 µm] and average for the four LMPL experiments. The mean values of F_{liq} are indicated in legend.

The shape classification performed by the CPI is presented Figure 6.a. The high droplet concentrations of the smallest CPI classes observed on March 11th and 29th (see Figure 5) are responsible of the strong number dominance of the droplets with a value of around 85 %. However, liquid water represents a very small proportion in mass and surface fractions. For these two quantities, side planes and irregular shapes dominate.

The assessment of the crystal growth mode is confronted to the fact that the measurement station can change its position in the cloud. An evolution in the CPI PSD is so not necessary due to particles growth. However, the crystal shape, accurately measured by the CPI, is a good indicator for the growth mode and the high percentage of regular shape would indicate a growth dominated by vapor deposition. Aircraft measurements performed in Svalbard in 2007 show similar results, with in particular strong presence of irregulars and side planes for altitudes and temperatures around 500 m and -12 °C, respectively (Gayet et al., 2009)

Atmos. Chem. Phys. Discuss., https://doi.org/10.5194/acp-2017-672
Manuscript under review for journal Atmos. Chem. Phys.
Discussion started: 1 November 2017

Atmospheric Chemistry and Physics Discussions

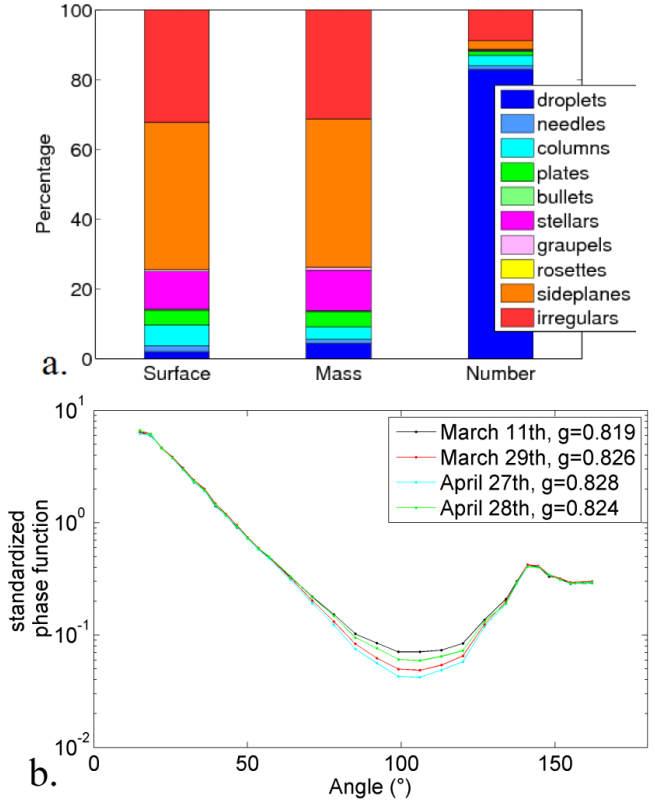

Figure 6: a) CPI shape classification in surface, mass and number for the LMPL cases. The color represents the occurrence percentage of the shapes as indicated by caption, and b) average standardized phase functions measured by the PN for the four LMPL cases. Caption indicates the asymmetry parameter.

Measurements of the cloud particle scattering properties performed by the PN allow to study the optical signature of the main microphysical properties observed on the MPC. Figure 6.b displays the average phase functions and asymmetry parameters (g) for the four LMPL cases. Differences between the experiments are negligible in forward and backward scattering but within the lateral scattering domain [60°; 130°]. The scattering increases when g decreases. The 1 minute average g values during the whole measurement campaign are included between 0.74 and 0.85, which is consistent with results obtained by Garrett et al. (2001).

Combined with Figure 5, these results show that g and the lateral scattering are relied to microphysical properties. Indeed, lateral diffusion increases when F_{liq} decreases. Therefore, March 11th experiment presents the lower F_{liq} (38 %), the higher lateral scattering and the lower average value of g (0.819). The contrary is shown in the April 27th case (F_{liq} = 94%, g = 0.828). This is consistent with previous studies (Gayet et al., 2009; Jourdan et al., 2010) and also proves the qualitative coherence between the FSSP and the PN.

The analysis of the optical-microphysics coupling is limited by the sampling speed and rate and the PN measurement accuracy. Indeed, a mean component analysis failed to establish a relationship between the phase function and the crystal morphology, as highlighted by Jourdan et al. (2010).

Atmos. Chem. Phys. Discuss., https://doi.org/10.5194/acp-2017-672
Manuscript under review for journal Atmos. Chem. Phys.
Discussion started: 1 November 2017

Atmospheric Chemistry and Physics Discussions

3.3 Characterization of the precipitation cases

Figure 7 displays the average CPI PSD for the three cases of precipitation. The FSSP is blind for those particles sizes. The April 14th and 20th experiments show a PSD with very low concentrations, close to the detection limit, centered around 350 µm and accompanied by relatively low temperature < -10°C. The March 28th case differs from the two other experiments with higher concentrations and a PSD centered around 200 µm, similar to the LMPL cases. Besides, the temperature is higher with an average value of -5 °C. This could reveal an influence of the mixed layer and/or temperature effect.

However, the ceilometer located the cloud base at an altitude of approximately 1000 m for the three days, which would indicate that the station position doesn't explain the differences. The temperature differences could lead to different growth processes and so different sizes.

This information can be provided by the CPI image classification presented Figure 8.a showing a pronounced presence of stellars. Even if the stellar crystals aren't a majority in number, they stand for more than half of total surface and mass. However, the number shape distribution was not identical for the three days. Indeed, the 14th and 20th April experiments are dominated by stellar whereas the March 28th case shows a much more important contribution of plaque, irregular and needle. As the concentration is 5 times higher for the March 28th case, its contribution in the total number distribution is more important.

Therefore, even if the temperature measured at the station is potentially different than the crystal formation and growth temperatures and the oversaturation according to the ice was not measured, we have seen that the CPI measurements show that temperatures below -10°C are favorable to the formation of big size crystals such as stellar, whereas, for warmer temperatures, plaque, irregular and needle crystals with smaller sizes dominate. This agrees with the crystal classification studied by Bailey and Halley (2009) and explains the differences in the daily PSD.

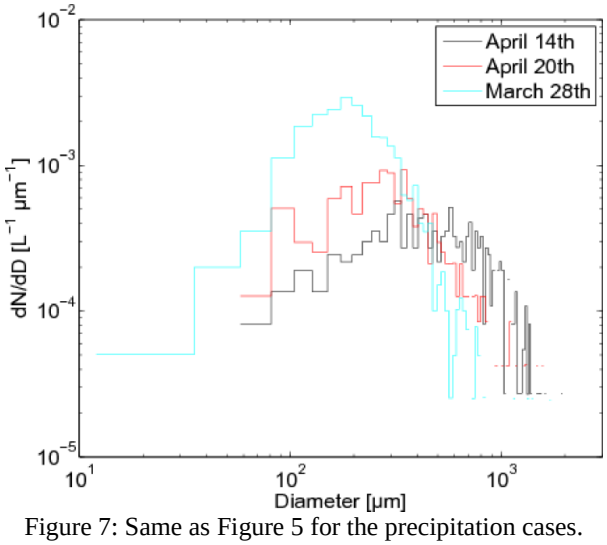

Figure 7: Same as Figure 5 for the precipitation cases.

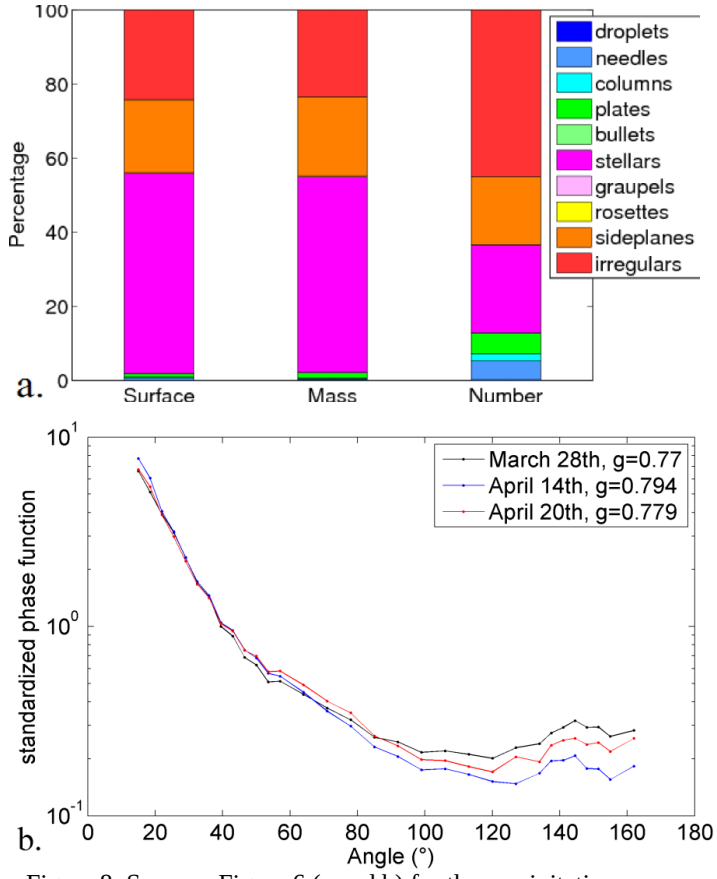

Figure 8: Same as Figure 6 (a and b) for the precipitation cases.

Figure 8.b presents the average phase functions of the precipitation cases. The lateral scattering is more important than for the measurements of the mixed and liquid layers. The asymmetry parameter is lower around 0.79 which is typical for ice particles. Notable differences are observed for scattering angles as low as 40°. These differences are probably due to the crystal morphology variability. Unfortunately, such relationships were not observed with the CLIMSLIP data. Indeed, a principal component analysis didn't allow discriminating the phase function according to the crystal shape. This can be explained by the low sampling rate during the precipitation events involving a very low crystal statistics.

To conclude, the results were limited by the low particle sampling rate and the uncontrolled position of the station inside the cloud system. However, differences between LMPL and precipitation layer have been explicated and allow a quick recognition without visual observations in future studies. These results will be compared to other measurement campaign for a better understanding of the microphysical processes and feedbacks that take place in low level mixed phase arctic clouds.

Atmos. Chem. Phys. Discuss., https://doi.org/10.5194/acp-2017-672
Manuscript under review for journal Atmos. Chem. Phys.
Discussion started: 1 November 2017

Atmospheric Chemistry and Physics Discussions

4 Aerosol-cloud interaction in the Arctic

The objective of this part is to quantify the effects of the aerosol properties on the cloud properties observed during the CLIMSLIP campaign. To do this, we will in a first step compare the two experiments of March 11th and 29th that will be the "clean" and "polluted" cases, respectively. In a second step, several aerosol cloud-interaction processes will be evaluated and in situ measurements will be used to assess quantities that are required in parametrization of the arctic aerosol-cloud interaction.

4.1 Section on tools: the FLEXPART-WRF model and definitions

This analysis will be supported by results from the lagrangian particle dispersion model FLEXPART-WRF (version 3.1, Brioude et al., 2013) adapted from the FLEXPART model (version 6.2, Stohl et al., 2005). FLEXPART-WRF simulates long distance transport and, in a mesoscale, the moist and dry scavenging and the diffusion of atmospheric tracers and air masses (see Stohl et al., 1998, Stohl and Thomson, 1999, or Stohl et al., 2005, for more details). The FLEXPART-WRF model was driven by WRF (Skamarock et al., 2008) meteorological forecasts to provide air masses back-trajectories and several tracers' origins.

For each single run, 20000 pseudo-particles were released from a small volume surrounding the analyzed position. Then, they were then tracked backward in time. The model output a tridimensional distribution of the Potential Emission Sensitivity (PES) on a 1° longitude x 1° latitude resolution grid. The PES is expressed in s/kg, which corresponds to the residence time of air particles within a given cell. In order to investigate the potential sources of the pollution transported to the Arctic and since the pollutants generally remain below the inversion layer, the model output is integrated over the first kilometer atmospheric column and becomes a Footprint PES (FPES). Combined with the ECLIPSE (Evaluating the Climate and Air Quality Impacts of Short-Lived Pollutants, see Klimont et al., 2016) atmospheric pollutants emission inventory, FLEXPART-WRF provides a valuable insight on the potential geographic contribution of anthropogenic sources for pollution tracers such as CO, SO_2 and BC. The combination between the FPES and the emissions is called the Potential Source Contribution (PSC) expressed in kg of tracer per air kg. In this study, we will focus on the CO tracer which gives an assessment on the origin of the anthropogenic pollution transported to Svalbard.

The aerosol cloud interaction study will also be supported by two other parameters: the activation fraction F_a and the activation diameter D_a. F_a can be defined as the percentage of aerosols becoming CCN (Abdul-Razzak et al., 1998) and is computed by the ratio of the FSSP and CPC concentration. The CPC was chosen because it provides the largest aerosol size range:

$$F_a = \frac{N_{drop}}{N_{aerosol}} = \frac{N_{FSSP}}{N_{CPC}} \quad (2)$$

We define D_a as the diameter beyond which all the aerosols are activated, assuming the aerosol chemistry effect is negligible (Abdul-Razzak et al., 1998). During CLIMSLIP, D_a is calculated as the DMPS diameter for which the DMPS total concentration is equal to the FSSP concentration. Even if the aerosol size range is smaller for the DMPS than the CPC, the DMPS was chosen because the aerosol PSD is necessary:

Atmos. Chem. Phys. Discuss., https://doi.org/10.5194/acp-2017-672
Manuscript under review for journal Atmos. Chem. Phys.
Discussion started: 1 November 2017

Atmospheric Chemistry and Physics Discussions

$$\sum_{D_{max}}^{D_a} n_{DMPS}(D) = N_{FSSP} \quad (3)$$

4.1 The "Clean" case of March 11th

The March 11th case, just like March 29th, presents a stable atmosphere with a low level mixed phase cloud. The liquid layer was sampled but, unfortunately, the ceilometer beam was almost entirely attenuated within the first 500 meters, avoiding to assess cloud top and base altitude. The sounding balloon show the inversion layer around 925 mb (700 m) for both days.
Figure 9 shows the time evolution of the DMPS, CPC and FSSP concentration, the activation fraction and the average BC concentration. The DMPS ceased to work from 7:30 until the following day, but, as the CPC and aethalometer parameters show almost constant values until 12:00, the DMPS concentration is assumed to do the same. The DMPS concentration is plotted for different particles sizes (total, > 50 nm and > 100 nm). The DMPS PSD shows a bimodal distribution with a pronounced Aitken mode which is as important as the accumulation mode (not shown). This is obvious in Figure 9 where the accumulation mode concentration, i.e. particles sizes larger than 100 nm, equals half the total concentration.
The CPC displays an aerosol concentration (> 3 nm) relatively stable and weak between 100 and 130 cm^{-3}. The average BC concentration reaches 22.6 ng m^{-3} during the liquid episode. The FSSP shows a droplet concentration up to 100 cm^{-3}, which leads to F_a values between 60 and 80 % for the sections clearly in the densest zone of the MPC liquid layer.
The FSSP droplet effective diameter is around 12 µm and the DMPS effective diameter around 250 µm. D_a shows very high variations with a mean value around 150 nm (not shown).

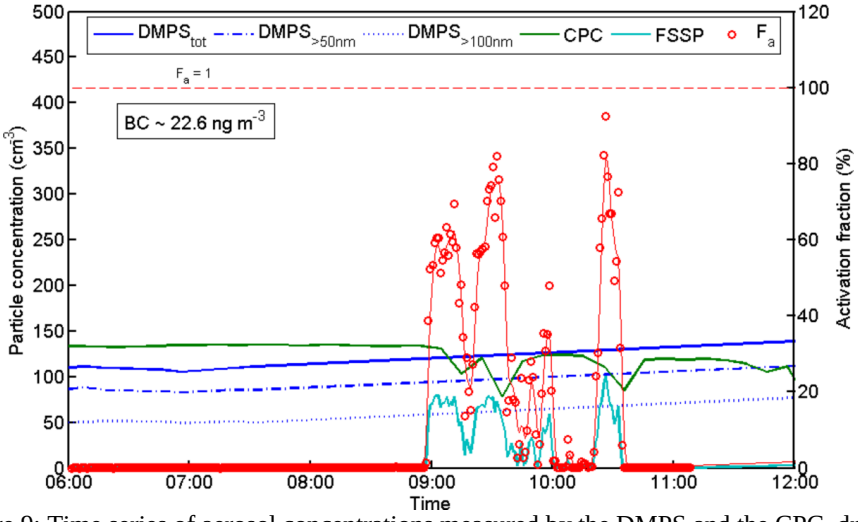

Figure 9: Time series of aerosol concentrations measured by the DMPS and the CPC, droplet FSSP concentration and the activation fraction, for the March 11th. The DMPS concentration was divided into three groups: the total concentration [25 - 809 nm], particles larger than 50 nm [50 – 809 nm] and larger than 100 nm [100 – 809 nm], the latter corresponding to the accumulation mode concentration. The activation fraction has been plotted with a sliding average of 5 minutes; the average aethalomètre BC concentration is indicated.

Atmos. Chem. Phys. Discuss., https://doi.org/10.5194/acp-2017-672
Manuscript under review for journal Atmos. Chem. Phys.
Discussion started: 1 November 2017

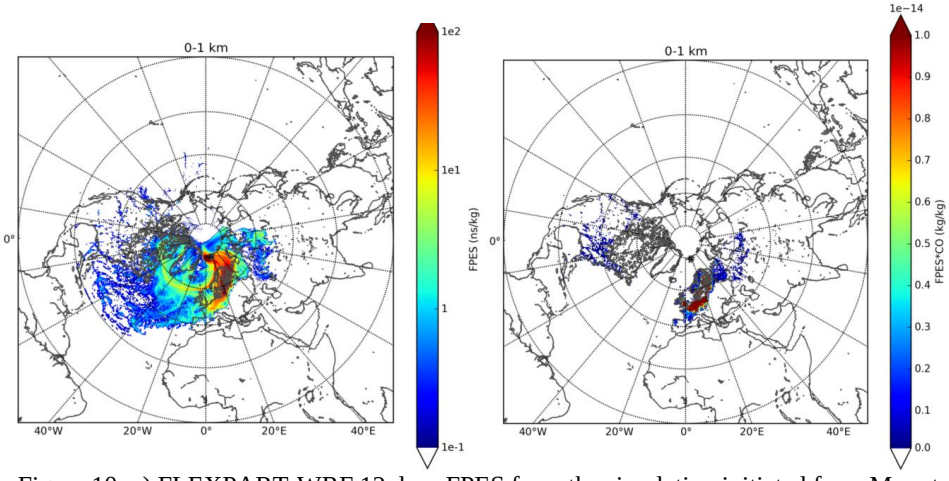

Figure 10: a) FLEXPART-WRF 12 days FPES from the simulation initiated from Mount-Zeppelin on March 11th between 9 AM and 12 AM UTC. b) PSC computed from the FPES of Figure a) for the CO, expressed in kg CO per kg air.

Figures 10 a and b present respectively the FPES over 12 days and the PSC of CO for the air mass arriving at the station during the liquid episode of the March 11th described in Figure 9. The FPES shows that the aerosol sources are mainly located in the north of Scandinavia and so that the long-range transport of anthropogenic aerosols is relatively limited. Indeed, over the FLEXPART-WRF time computation of 12 days, the air masses come principally from Svalbard and Scandinavia surrounding, showing very slow move. The CO PSC map presents an anthropogenic origin dominated by North Europa: Scandinavia, north of Germany, Netherland, Belgium and north of France.
The closer air masses origin makes this case the "clean" case. The important contribution of local aerosol sources, mainly composed of gaseous precursors for the arctic region during this period of the year (Quinn et al., 2007), explains the relative small aerosol mean diameter and the high Aitken mode concentration observed by the DMPS (see Figure 9).

4.2 The "Polluted" case of March 29th

Figure 11 displays the same time series as Figure 9 for the liquid episode of March 29th. The CPC and DMPS total concentration are decreasing going respectively from 220 cm^{-3} to 120 cm^{-3} and from 175 cm^{-3} to 80 cm^{-3}, due to the scavenging by ice precipitation. The FSSP droplet concentrating reaches 150 cm^{-3} and the average BC concentration 65.8 ng m^{-3}. Comparing to the March 11th case, these four concentration are all higher during the March 29th. The activation fraction is also higher on March 29th with values between 80 and 100 % in the liquid layer and F_a increases as the aerosol concentration decreases.
Just like March 11th, D_a shows very variable values around 150 nm (not shown). Its high variability makes this parameter unsuitable when comparing the two cases. However, D_a decreases from around 150 nm to 50 nm and the FSSP effective diameter increases from 8 to 10 µm when F_a increases, proving that smaller aerosol particles are activated and droplets grow when the aerosol number decreases.

Atmos. Chem. Phys. Discuss., https://doi.org/10.5194/acp-2017-672
Manuscript under review for journal Atmos. Chem. Phys.
Discussion started: 1 November 2017

Atmospheric Chemistry and Physics Discussions

Moreover, the DMPS PSD shows that 90 % of the aerosol concentration is included in the accumulation mode, with an effective diameter almost constant at 300 nm. Therefore, the aerosol diameter is larger and the droplet diameter is smaller for the March 29th case compared to the March 11th case.

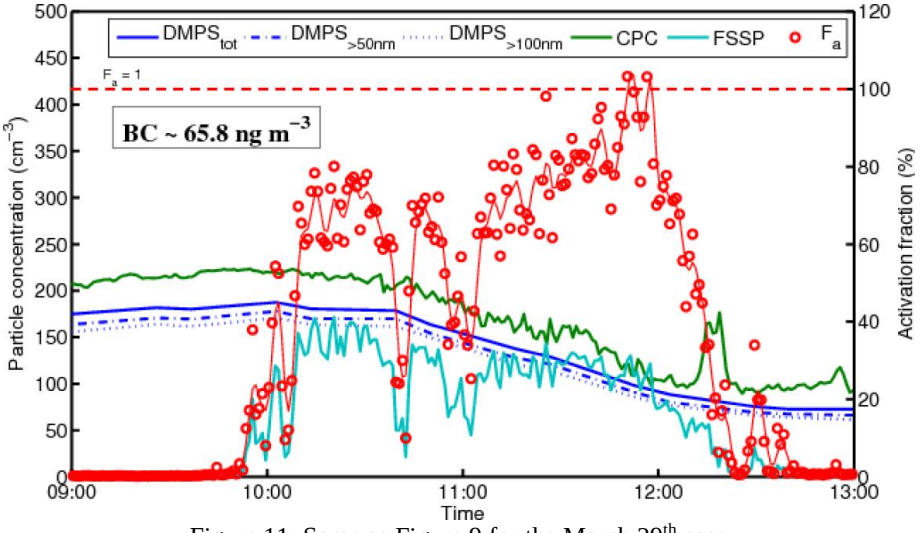

Figure 11: Same as Figure 9 for the March 29th case

The differences observed between the two days can be explained by the air masses origin. Figure 12 shows the same FLEXPART-WRF FPES and CO PSC for the air mass arriving at the station during the liquid episode of the March 29th. Backtrajectories distinguish clearly two origin regions. The first one is Western Europa. The second air mass shows higher values of time residence and comes from northeast Asia: northeast China and extreme east Russia. The particularity of March 29th consists thus in this air mass coming from Asia which is the region generally accepted to emit the highest aerosol concentration compared to the others regions of the world (Boucher et al., 2013).

Therefore, compared to the "clean" case of March 11th, March 29th shows long range transport of anthropogenically influenced air masses, leading to higher aerosol concentration in the Arctic with especially a BC mass concentration 3 times higher. Thus, March 29th constitute the "polluted" case. According to Quennehen et al. (2012), during the route, the Aitken mode concentration quickly decreases by coagulation, for the benefit of the accumulation mode, increasing the average effective diameter. This explains the accumulation mode dominance observed in Figure 11 and the increase of the average DMPS effective diameter, and confirms the strong influence of the lower latitudes emissions during the "polluted" case. On the contrary, the "clean" case shows local sources composed of fresh particles, for at least half the concentration.

This long range anthropogenic pollution has also strong influence on cloud properties. Indeed, CCN abilities being mainly due to the aerosol size in the Arctic (Mc Farquhar et al., 2011), accumulation mode dominance leads to higher aerosol effective diameter and higher F_a values. Combined with higher aerosol concentration, the droplet concentration increases whereas the droplet size decreases meaning, theoretically, that the cloud optical thickness increases.

Atmos. Chem. Phys. Discuss., https://doi.org/10.5194/acp-2017-672
Manuscript under review for journal Atmos. Chem. Phys.
Discussion started: 1 November 2017

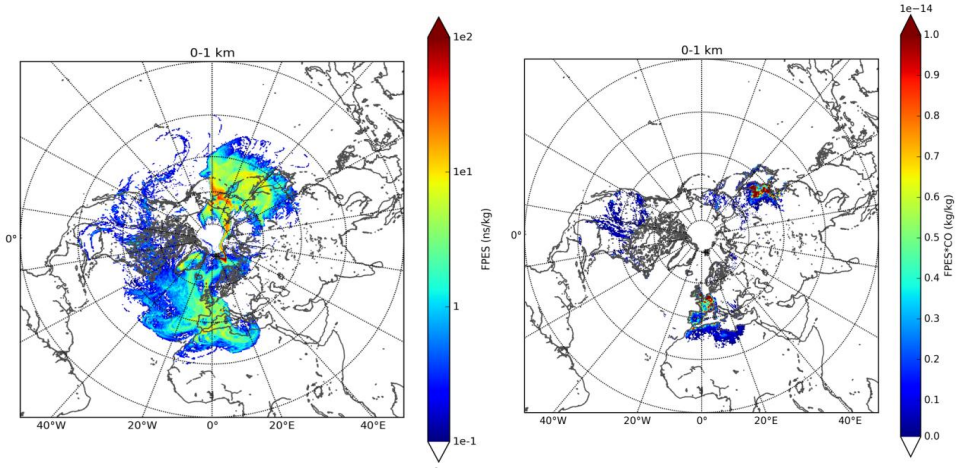

Figure 12: a) and b) Same as Figure 10 for the air masses arriving in the Mount-Zeppelin station on March 29th between 10 AM and 1 PM UTC.

This qualitative study has to be completed with quantitative parameters that can be found in the scientific literature. Therefore, the next section will focus on the quantitative variations of droplet concentration and size according to aerosol properties. Moreover, glaciation and riming indirect effect will be assessed.

4.3 Quantification of the impacts of the aerosol properties on the cloud microphysical properties

The sensitivity of cloud diameter and concentration according to aerosol haze will be assessed from two parameters, called the Indirect Effect parameter (*IE*) and the Nucleation Efficiency (*NE*) and defined as follows (Feingold et al., 2001, 2003, Garrett et al., 2004):

$$IE = -\frac{\partial \ln(r_e)}{\partial \ln(\sigma)} \quad (4)$$

$$NE = \frac{\partial \ln(N)}{\partial \ln(\sigma)} \quad (5)$$

where r_e is the droplet effective radius, N the droplet concentration and σ the aerosol scattering coefficient.

We made two assumptions to use these parameters. First, *IE* and *NE* are assumed to evaluate the variations of the droplet concentration and size according to the CCN concentration. To measure this one, we use the scattering coefficient which is assumed to be proportional to the CCN concentration. The accumulation mode particles are the most inclined to serve as CCN because of their size and possess the highest scattering cross section compared to the other modes (Garrett et al., 2004). Second, r_e and N are also dependent on the *LWP*, so *IE* and *NE* have to be computed for similar *LWP* clouds (Feingold et al., 2001). During CLIMSLIP, the *LWP* was not measured and we assumed that the *LWP* is effectively constant. This is reasonable since the sampled clouds were all low level mixed phase arctic clouds and from the same season.

Atmos. Chem. Phys. Discuss., https://doi.org/10.5194/acp-2017-672
Manuscript under review for journal Atmos. Chem. Phys.
Discussion started: 1 November 2017

Atmospheric Chemistry and Physics Discussions

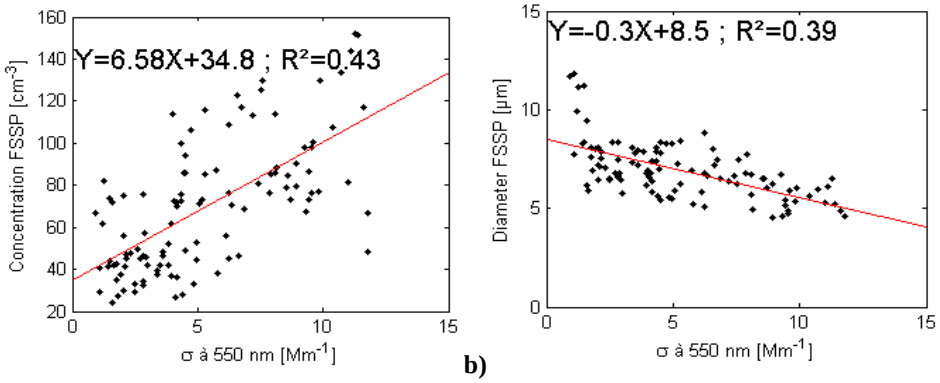

a) **b)**

Figure 13: Comparison of the aerosol scattering coefficient σ at λ = 550 nm measured by the nephelometer, with a) the droplet concentration, and b), the effective diameter measured by the FSSP, for the four LMPL cases. Values of *LWC* below 5 10^{-3} g m^{-3} were not taken into account. This comparison has been performed with a nephelometer time resolution of 5 minutes.

Figure 13 presents the comparisons between the droplet concentration and diameter with the aerosol scattering coefficient. The results are consistent with the Twomey effect (Twomey, 1974, 1977) and the Albrecht effect (Albrecht, 1989). The correlation coefficients R^2 are equal to 0.43 and 0.39 for concentration and size, respectively. This high dispersion can be explained by the fact that the droplet concentration and size depend also of *LWP*, temperature and the position of the measurement volume within the cloud system.
At λ = 550 nm, *IE* = 0.2 and *NE* = 0.43 were obtained. This is to compare with the study of Garrett et al. (2004) performed at Barrow, Alaska, where *IE* and *NE* were found to be between 0.13 and 0.19 and between 0.3 and 0.5 respectively, at λ = 550 nm. Very similar values are so found in two different regions of the Arctic, which confirms these parameterizations of the first and second aerosol indirect effect for the arctic region.

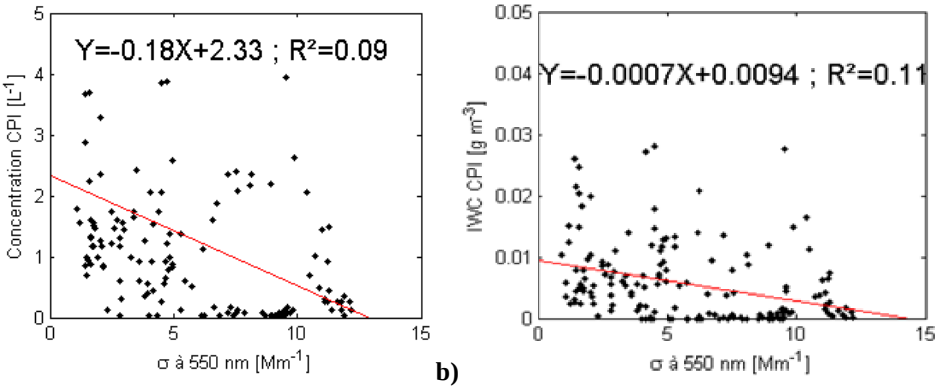

a) **b)**

Figure 14: 5 minutes comparison of the aerosol scattering coefficient σ at λ = 550 nm with a) the concentration and b) the *IWC* of crystals sampled by the CPI, for the four LMPL cases. A threshold of 50 µm was applied to the particles diameter to discard the droplets sampled by the CPI.

The glaciation (Lohmann, 2002a, 2002b) and the riming indirect effect (Borys et al., 2003) were evaluated during the CLIMSLIP campaign thanks to the CPI and the nephelometer measurements. The comparison between the crystal concentration and *IWC* with σ (or nuclei concentration) is displayed in Figure 14. The results show very weak correlation, for the concentration and the *IWC*. This means that neither the glaciation nor the riming indirect effect were revealed during CLIMSLIP.

This absence can be due to the high uncertainty in the CPI measurements and/or to low sampling rate that leads to a very low statistical representation. To compare, the study of Jackson et al. (2012), during the ISDAC and MPACE campaign, found a correlation corresponding to the glaciation effect above the cloud liquid phase but no evidence of the riming effect.

5 Summary and conclusion

Within the framework of the arctic amplification, the complex interactions between the cloud and aerosol properties remain a challenge to enhance the arctic cloud modeling and to get a better quantification of the consequences of the anthropogenic pollution on the arctic climate. The ANR project CLIMSLIP (CLimate IMpacts of Short-LIved Pollutants in the polar region) provides new data from a ground based aerosol and cloud instrumentation located at the Mount Zeppelin station, Ny-Alesund, Svalbard, during spring 2012. This instrumentation contains a FSSP, a CPI and a Polar Nephelometer to sample clouds and a CPC, a DMPS and a nephelometer for aerosols.

During the campaign, four cases of LMPL (Liquid and Mixed Phase Layer), three cases of snow precipitation layer and two cases of BS (Blowing Snow) were sampled. The precipitation layer cases correspond to the lower layer of a MPC. The precipitation events are composed of large crystals (Mean Diameter $Dm \sim 350$ µm) with an important presence of stellar. The LMPL events are characterized by a bimodal PSD with a large number of droplets. The liquid mode was located around 10 µm and the crystal mode around 250 µm. The phase function measurements showed an increase of the lateral scattering as F_{liq} decreases.

According to Guyot et al. (2015), only isoaxial measurements with a wind speed higher than 5 m/s are selected. This deleted a non-negligible amount of data and so limited the analysis, especially for the precipitation cases where the particle statistics were the weaker. Moreover, the position of the station within the cloud system was approximate despite the ceilometer measurements.

A study by comparison of the effects of the anthropological aerosols transported to the Arctic was performed. According to the FLEXPART/WRF simulations, the "polluted" case of March 29th showed air masses from Europe and East Asia whereas the aerosol sources during the "clean" case of March 11th were closer (mainly from Scandinavia) and the anthropogenic contribution doesn't exceed northern Europe.

Thus, the polluted case presents higher Black Carbon, aerosol and droplets concentrations, a more important accumulation mode, smaller droplet sizes and higher activation fraction F_a. The March 29th activation diameter D_a decreased when the droplet diameter increased and F_a increased, proving that smaller aerosol particles are activated and droplets grow up when the aerosol number decreases. These results confirm the first and second aerosol indirect effects with the coefficients *IE* and *NE* respectively around 0.2 and 0.43. These values are very close to those found by Garrett et al. (2004), which performed measurement at Barrow in Alaska, and are so good candidates to be used to parameterize arctic aerosol-cloud interaction in climate models. Furthermore, the crystal concentration and *IWC* do not show any correlation with the aerosol properties, which indicates that the glaciation and riming indirect effects are not highlighted during the CLIMSLIP-NyA campaign.

Acknoledgements. This work was supported by the ANR project CLIMSLIP and the conseil general de l'Allier. We also thank the AVI for providing the ceilometer data and the ITM and NILU for monitoring the Mount Zeppelin station. We are grateful to scientists, engineers and technicians that make this study possible. Boris Quennehen acknowledges the IPSL CICLAD/CLIMSERV mesocenter for providing computing resources.

Atmos. Chem. Phys. Discuss., https://doi.org/10.5194/acp-2017-672
Manuscript under review for journal Atmos. Chem. Phys.
Discussion started: 1 November 2017

Atmospheric Chemistry and Physics Discussions

Annex: Characterization of the Blowing Snow (BS) cases

During ground based measurements, some snow was collected that was suspended in the atmosphere due to wind. This is the so-called Blowing Snow (BS). This annex aims at the microphysics characterization in order to recognize this kind of episode and the optical properties measurements, especially the phase function, that can be used as a reference to develop new parameterizations of the snow simple scattering properties (Räisänen et al., 2015).

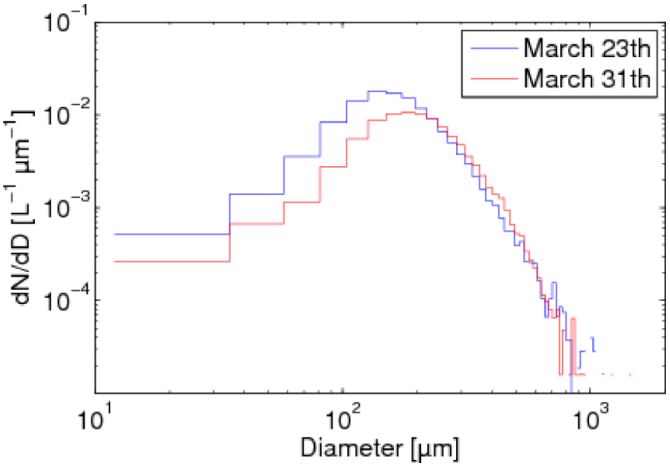

Figure 15: Same as Figure 5 for the BS cases.

When the BS occurs, the sky is clear as observed by the ceilometer. However, crystal particles are sampled. They are snowflakes initially resting on the ground but getting suspended in the air by the wind.

Figure 15 shows the average PSDs measured by the CPI for the two BS cases. The shape and the amplitude are similar for the two PSDs, with a mean diameter between 150 and 200 µm. for a maximum class concentration around 10^{-2} L^{-1} µm^{-1}. The CPI shape classification, plotted in Figure 16.a, shows a large prevalence of irregular crystals, as well in number, surface or mass (i.e. volume), with a percentage around 90% of the crystals. These two characteristics constitute the microphysics signature of the BS. The difference between the BS and MPC (see Figure 5 and 6) signature makes it possible to identify BS events even if the station is located inside a cloud.

Atmos. Chem. Phys. Discuss., https://doi.org/10.5194/acp-2017-672
Manuscript under review for journal Atmos. Chem. Phys.
Discussion started: 1 November 2017

Atmospheric Chemistry and Physics Discussions

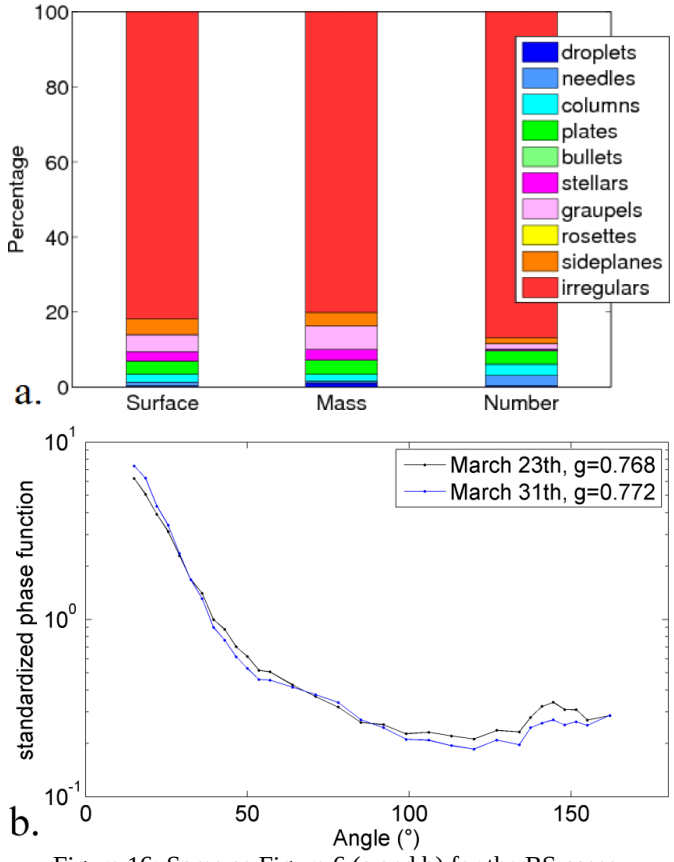

Figure 16: Same as Figure 6 (a and b) for the BS cases.

Even if the resuspension of crystals in the air can modify the shape by impacts, we consider that the sampled crystals are similar to the deposited precipitations and aged for several days. Thus, the BS events during CLIMSLIP were excellent occasions to measure the arctic snow properties.

Figure 16.b displays the average phase functions of the BS cases. The shape of the curves are very similar to the precipitation cases, typical of ice particles, but with lower *g* values. These measurements constitute a unique database to develop parameterizations of the arctic snow optical properties. Indeed, in most of the climate and weather forecast models, the computation of the snow albedo uses the approximation of spherical snow grain (Wang and Zeng, 2010). Thus, the study of Räisänen et al. (2015) proposes new modeling parameterizations of the snow single scattering properties (SSP) based on the CLIMSLIP-NyA in situ measurement of the phase function. The obtained snow SSP takes into account the complex BS particles shape (Räisänen et al., 2015).

References

Abdul-Razzak, H., Ghan, S. and Rivera-Carpio, C.: A parametrization of aerosol activation; 1. Single aerosol type, J. Geophys. Res., 103, 6123-6131, 1998.

Albrecht, B.A.: Aerosols, cloud microphysics, and fractional cloudiness, Science, 245, 1227-1230, 1989.

Bailey, M. P., and Hallett, J.: A Comprehensive Habit Diagram for Atmospheric Ice Crystals: Confirmation from the Laboratory, AIRS II, and Other Field Studies, J. Atmos. Sci., 66, 2888–2899, doi:10.1175/2009JAS2883.1, 2009.

Baker, B. and Lawson, R.P.: Improvement in Determination of Ice Water Content from Two-Dimensional Particle Imagery. Part I: Image-to-Mass Relationships. J. Appl. Meteor. Climatol., 45, 1282–1290, 2006.

Borys, R.D., Lowenthal, D.H., Cohn S.A. and Brown, W.O.J.: Mountaintop and radar measurements of anthropogenic aerosol effects on snow growth and snowfall rate, Geophys. Res. Lett., 30, 1538, doi:10.1029/2002GL016855, 2003.

Boucher, O., Randall, D., Artaxo, P., Bretherton, C., Feingold, G., Forster, P., Kerminen, V.-M., Kondo, Y., Liao, H., Lohmann, U., Rasch, P., Satheesh, S.K., Sherwood, S., Stevens B. and Zhang, X.Y.: Clouds and Aerosols. In: Climate Change 2013: The Physical Science Basis. Contribution of Working Group I to the Fifth Assessment Report of the Intergovernmental Panel on Climate Change, Cambridge University Press, Cambridge, United Kingdom and New York, NY, USA, 2013.

Brioude, J., Arnold, D., Stohl, A., Cassiani, M., Morton, D., Seibert, P., Angevine, W., Evan, S., Dingwell, A., Fast, J. D., Easter, R. C., Pisso, I., Burkhart, J., and Wotawa, G.: The Lagrangian particle dispersion model FLEXPART-WRF version 3.1, Geosci. Model Dev., 6, 1889–1904, doi:10.5194/gmd-6-1889-2013, 2013.

Costa, A., Krämer, M., Meyer, J., Afchine, A., Luebke, A., Dorsey, J.R., Gallagher, M.W., Ehrlich, A., Wendisch, M., Baumgardner, D., Möhler, O., Saathoff, H. and Schnaiter, M.: A microphysical classification of mixed-phase clouds in the liquid-ice coexistence and Wegener-Bergeron-Findeisen regime, 14th Conference on Cloud Physics, 07 – 11 July 2014, Boston, USA, https://ams.confex.com/ams/14CLOUD14ATRAD/webprogram/Handout/Paper250419/AMS_Poster_68_Mixed_Phase_Clouds_Costa.pdf, 2014.

Curry, J.A., Randall, D., Rossow, W.B., and Schramm, J.L.: Overview of Arctic Cloud and Radiation Characteristics, J. Climate, 9, 1731–1764, doi: 10.1175/1520-0442(1996)009<1731:OOACAR>2.0.CO;2, 1996.

Dufresne, J.L. and Bony, S. : An Assessment of the Primary Sources of Spread of Global Warming Estimates from Coupled Atmosphere–Ocean Models, J. of Clim., 21, 5135 – 5144, 2008.

Dye, J.E., Baumgardner D.: Evaluation of the Forward Scattering Spectrometer Probe. Part I: Electronic and Optical Studies, J. Atmos. Oceanic Technol., 1, 329-344, 1984.

841 Eleftheriadis, K., Vratolis, S. and Nyeki, S.: Aerosol black carbon in the European Arctic:
842 Measurements at Zeppelin station, Ny-Alesund, Svalbard from 1998–2007, Geophys. Res.
843 Lett., 36, L02809, doi:10.1029/2008GL035741, 2009.
844
845 Engvall, A.C., Krejci, R., Ström, J., Treffeisen, R., Scheele, R., Hermansen, O. and Paatero, J.:
846 Changes in aerosol properties during spring-summer period in the Arctic troposphere, Atmos.
847 Chem. Phys., 8, 445-462, 2008.
848
849 Febvre G., Gayet, J.F., Shcherbakov., V., Gourbeyre, C., Jourdan, O.: Some effects of ice
850 crystals on the FSSP measurements in mixed phase clouds, Atmos. Chem. Phys., 12, 8963–
851 8977, doi: 10.5194/acp-12-8963-2012, 2012.
852
853 Feingold, G., Remer, L. A., Ramaprasad, J., and Kaufman, Y. J.: Analysis of smoke impact on
854 clouds in Brazilian biomass burning regions: An extension of Twomey's approach, J. Geophys.
855 Res., 106, 22, 907– 22, 922, 2001.
856
857 Feingold, G., Eberhard, W. L., Veron, D. E. and Previdi, M.: First measurements of the
858 Twomey indirect effect using ground-based remote sensors, Geophys. Res. Lett., 30, 1287, doi:
859 10.1029/2002GL016633, 2003.
860
861 Garrett, T. J., Hobbs, P. V., and Gerber, H.: Shortwave, single scattering properties of Arctic
862 ice clouds, J. Geophys. Res., 106, 15 155–15 172, 2001.
863
864 Garrett, T. J., Zhao, C. Dong, X., Mace, G., Hobbs, P. V.: Effects of Varying Aerosol Regimes
865 on Low-Level Arctic Stratus. Geophys. Res. Lett., 31, 17, 17, doi: 10.1029/2004GL019928,
866 2004.
867
868 Garrett, T. and Zhao, C.: Increased Arctic cloud longwave emissivity associated with pollution
869 from mid-latitudes, Nature, 440, 787–789, doi:10.1038/nature04636, 2006.
870
871 Gayet, J.F., Crépel, O., Fournol, J.F., and Oshchepkov, A.: A new airborne polar nephelometer
872 for the measurements of optical cloud properties. Part I: Theoretical design, Ann. Geophysicae,
873 15, 451-459, 1997.
874
875 Gayet, J.F., Auriol, F., Minikin, A., Ström, J., Seifert, M., Krejci, R., Petzol, A., Febvre, G.,
876 and Schuman, U.: Quantitative measurement of the microphysical and optical properties of
877 cirrus clouds with four different in situ probes: Evidence of small crystals, Geo. Resea. Let.,
878 29, 2230-2233, 2002.
879
880 Gayet, J.F., Mioche, G., Dörnbrack, A., Ehrlich, A., Lampert, A., Wendisch M.: Microphysical
881 and optical properties of Arctic mixed-phase clouds. The 9 April 2007 case study, Atmos.
882 Chem. Phys., 9, 6581–6595, 2009.
883
884 Guyot, G., Gourbeyre, C., Febvre, G., Shcherbakov, V., Brunet, F., Dupont, J.C., Sellegri, K.
885 and Jourdan, O.: Quantitative evaluation of seven optical sensors for cloud microphysical
886 measurements at the Puy-de-Dôme Observatory, France, Atmos. Meas. Tech., 8, 4347–4367,
887 doi:10.5194/amt-8-4347-2015 , 2015.
888
889 Jackson, R.C., McFarquhar, G.M., Korolev, A.V., Earle, M.E., Liu, P.S.K., Lawson, R.P.,
890 Brooks, S., Wolde, M., Laskin, A. and Freer, M. : The dependence of ice microphysics on

aerosol concentration in arctic mixed-phase stratus clouds during ISDAC and M-PACE, J. Geophys. Res., 117, D15207, doi:10.1029/2012JD017668, 2012.

Jourdan, O., Mioche, G., Garrett, T.J., Schwarzenböck, A., Vidot, J., Xie, Y., Shcherbakov, V., Yang, P. and Gayet, J.F.: Coupling of the microphysical and optical properties of an Arctic nimbostratus cloud during the ASTAR 2004 experiment: Implications for light- scattering modeling, J. Geophys. Res., 115, D23206, doi:10.1029/2010JD014016, 2010.

Kay, J. E., Holland, M. M., Bitz, C. M., Blanchard-Wrigglesworth, E., Gettelman, A., Conley, A. and Bailey, D.: The Influence of Local Feedbacks and Northward Heat Transport on the Equilibrium Arctic Climate Response to Increased Greenhouse Gas Forcing, J. Clim., 25(16), 5433–5450, doi:10.1175/JCLI-D-11-00622.1, 2012.

Klimont, Z., Kupiainen, K., Heyes, C., Purohit, P., Cofala, J., Rafaj, P., Borken-Kleefeld, J., and Schöpp, W.: Global anthropogenic emissions of particulate matter including black carbon, Atmos. Chem. Phys. Discuss., https://doi.org/10.5194/acp-2016-880, in review, 2016.

Knollenberg, R.G.: Techniques for probing cloud microstructure, in: Clouds, their formation, optical properties and effects, Hobbs, P.V. and Deepak, A., Academic Press, New York, USA, 15-92, 1981.

Korolev, A.V., Strapp, J.W., Isaac, G.A. et Nevzorov, A.N.: The Nevzorov airborne hot wire LWC-TWC probe: Principe of operation and performance characteristics, J. Atmos. Ocean. Techn., 15, 1495-1510, 1998.

Korolev, A. V. and Isaac, G. A., Relative humidity in liquid, mixed-phase, and ice clouds, J. Atmos. Sci., 63, 2865–2880, 2006.

Lawson, R.P. and Baker, B.: Improvement in Determination of Ice Water Content from Two-Dimensional Particle Imagery. Part II: Applications to Collected Data. J. Appl. Meteor. Climatol., 45, 1291–1303, 2006.

Lefèvre, R. : Physique de la mesure de la sonde CPI pour la mesure des propriétés des cristaux de glace. Application aux observations réalisées durant la campagne ASTAR 2004, 186 p., Manuscrit de thèse, Université Blaise Pascal, 2007.

Lohmann, U.: Possible Aerosol Effects on Ice Clouds via Contact Nucleation, J. Atmos. Sci., 59, 647–656, , 2002a.

Lohmann, U.: A glaciation indirect aerosol effect caused by soot aerosols, Geophys. Res. Lett., 29, 1052-1056, doi:10.1029/2001GL014357, 2002b.

Mc Farquhar, G., Ghan, S. J., Verlinde, J., Korolev, A., Strapp, J. W., Schmid, B., Tomlinson, J., Wolde, M., Brooks, S., Cziczo, D., Dubey, M., Fan, J., Flynn, C., Gultepe, I., Hubbe, J., Gilles, M., Laskin, A., Lawson, P., Leaitch, W., Liu, P., Liu, X., Lubin, D., Mazzoleni, C., Mac Donald, A.M., Mo_et, R., Morrison, H., Ovchinnikov, M., Shupe, M., Turner, D., Xie, S., Zelenyuk, A., Bae, K, Freer, M., and Glen, A.: Indirect and semi-direct aerosol campaign: the impact of Arctic aerosols on clouds, B. Am. Meteorol. Soc., 92, 183–201, doi:10.1175/2010BAMS2935.1, 2011.

941 Mc Guire, D., Chapin, F.S., Walsh, J., Wirth, C.: Integrated regional changes in arctic climate
942 feedbacks: Implications for the Global Climate System, Annu. Rev. Environ. Resour., 31, 61–
943 91, doi: 10.1146/annurev.energy.31.020105. 100253, 2006.
944
945 Mioche, G., Jourdan, O., Ceccaldi, M., and Delanoë, J.: Variability of mixed-phase clouds in
946 the Arctic with a focus on the Svalbard region: a study based on spaceborne active remote
947 sensing, Atmos. Chem. Phys., 15, 2445-2461, doi:10.5194/acp-15-2445-2015, 2015.
948
949 Morrison, H., de Boer, G., Feingold, G., Harrington, J., Shupe, M.D., and Sulia, K.: Resilience
950 of persistent Arctic mixed-phase clouds, Nat. Geosci., 5, 11–17, doi:10.1038/ngeo1332, 2012.
951
952 Pincus, R. and Baker, M.: Effect of precipitation on the albedo susceptibility of clouds in the
953 marine boundary layer, Nature, 372, 250 – 252, doi: 10.1038/372250a0, 1994.
954
955 Quennehen, B., Schwarzenboeck, A., Matsuki, A., Burkhart, J. F., Stohl, A., Ancellet, G., and
956 Law, K. S.: Anthropogenic and forest fire pollution aerosol transported to the Arctic:
957 observations from the POLARCAT-France spring campaign, Atmos. Chem. Phys., 12, 6437–
958 6454, doi:10.5194/acp-12-6437-2012, 2012.
959
960 Quinn, P. K., Shaw, G.E. Andrews, E., Dutton, E.G., Ruoho-Airola, T. and Gong, L.: Arctic
961 haze: current trends and knowledge gaps, Tellus, 59, 99-114, 2007.
962
963 Quinn, P. K., Bates, T. S., Baum, E., Doubleday, N., Fiore, A. M., Flanner, M., Fridlind, A.,
964 Garrett, T. J., Koch, D., Menon, S., Shindell, D., Stohl, A., and Warren, S. G.: Short-lived
965 pollutants in the Arctic: their climate impact and possible mitigation strategies, Atmos. Chem.
966 Phys., 8, 1723-1735, doi:10.5194/acp-8-1723-2008, 2008.
967
968 Räisänen, P., Kokhanovsky, A., Guyot, G., Jourdan, O., Nousiainen, T.: Parameterization of
969 single-scattering properties of snow, The Cryosphere, 9, 1277–1301, doi:10.5194/tc-9-1277-
970 2015, 2015.
971
972 Rogers, D., Stith, J., Jensen, J., Cooper, W., Nagel, D., Maixner, U. and Goyea, O.: Splash
973 artifacts in FSSP measurements; observations and flow modeling studies, 12th conference of
974 cloud physics, Madison, USA, 10 – 14 July 2006, P2.30, 2006.
975
976 Screen, J.A. and Simmonds, I.: The central role of diminishing sea ice in recent Arctic
977 temperature amplification, Nature, 464, 1334-1337, doi:10.1038/nature09051, 2010.
978
979 Serreze, M. and Francis, J.: The arctic amplification debate, Climatic Change, 76, 241 – 264,
980 doi: 10.1007/s10584-005-9017-y, 2006.
981
982 Skamarock, W. C., J. B. Klemp, J. Dudhia, D. O. Gill, D. M. Barker, M. G Duda, X.-Y. Huang,
983 W. Wang, and J. G. Powers, 2008: A Description of the Advanced Research WRF Version 3.
984 *NCAR Tech. Note NCAR/TN-475+STR*, 113 pp.,
985 doi:10.5065/D68S4MVH, 2008.
986
987 Stohl, A., Hittenberger, M. and Wotawa, G.: Validation of the Lagrangian particle dispersion
988 model FLEXPART against large scale tracer experiments, Atmos. Environ., 32, 4245-4264,
989 1998.
990

991 Stohl, A. and Thomson, D.J.: A density correction for Lagrangian particle dispersion models,
992 Bound.-Layer Met., 90, 155-167, 1999.
993
994 Stohl, A., Forster, C., Frank, A., Seibert, P. and Wotaw, G.: Technical Note: The Lagrangian
995 particle dispersion model FLEXPART version 6.2, Atmos. Chem. Phys., 5, 2461-2474, 2005.
996
997 TSI: Model 3025A Ultrafine Condensation Particle Counter Instruction Manual, 2002.
998
999 TSI: Model 3563 Integrating Nephelometer Operation and Service Manual, 219 pp, 2005.
1000
1001 Tunved, P., Ström, J. and Krejci, R.: Arctic aerosol life cycle: linking aerosol size distributions
1002 observed between 2000 and 2010 with air mass transport and precipitation at Zeppelin station,
1003 Ny-Alesund, Svalbard, Atmos. Chem. Phys., 13, 3643–3660, doi:10.5194/acp-13-3643-2013,
1004 2013.
1005
1006 Twomey, S.: Pollution and the planetary albedo, Atmos. Environ., 8, 1251 – 1256, 1974.
1007
1008 Twomey, S.: The influence of pollution on the shortwave albedo of clouds, J. of Atmos.
1009 Sciences, 34, 1149 – 1152, 1977.
1010
1011 Uchiyama, A., Yamazaki, A., Shiobara, M. and Kobayashi, H. : Case study on microphysical
1012 properties of boundary layer mixed-phase cloud observed at Ny-Ålesund, Svalbard: Observed
1013 cloud microphysics and calculated optical properties on 9 June 2011, Polar Science, 8(2), 57–
1014 72, doi:10.1016/j.polar.2013.11.001, 2013.
1015
1016 Vaughan, D.G., Comiso, J.C., Allison, I., Carrasco, J., Kaser, G., Kwok, R., Mote, P., Murray,
1017 T., Paul, F., Ren, J., Rignot, E., Solomina, O. Steffen, K. and Zhang, T.: Observations:
1018 Cryosphere. In: Climate Change 2013: The Physical Science Basis. Contribution of Working
1019 Group I to the Fifth Assessment Report of the Intergovernmental Panel on Climate Change
1020 [Stocker, T.F., D. Qin, G.-K. Plattner, M. Tignor, S.K. Allen, J. Boschung, A. Nauels, Y. Xia,
1021 V. Bex and P.M. Midgley (eds.)]. Cambridge University Press, Cambridge, United Kingdom
1022 and New York, NY, USA, 2013.
1023
1024 Wang, Z. and Zeng, X.: Evaluation of snow albedo in land models for weather and climate
1025 studies, J. Appl. Meteorol. Clim., 49, 363–380, 2010.
1026
1027 Wendisch, M., Yang, P., and Ehrlich, A.: Amplified climate changes in the Arctic: Role of
1028 clouds and atmospheric radiation, vol. 132, 1–34, Sitzungsberichte der Sächsischen Akademie
1029 der Wissenschaften zu Leipzig, Mathematisch-Naturwissenschaftliche Klasse, S. Hirzel
1030 Verlag, Stuttgart/Leipzig, 2013.